p-n Junction Dynamics Induced in a Graphene Channel by Ferroelectric-Domain Motion in the Substrate

Anatolii I. Kurchak,[1] Eugene A. Eliseev,[2] Sergei V. Kalinin,[3] Maksym V. Strikha,[1,4,*] and Anna N. Morozovska[5,6,†]

[1]*V. Lashkariov Institute of Semiconductor Physics, National Academy of Sciences of Ukraine, Prospect Nauky 41, 03028 Kyiv, Ukraine*

[2]*Institute for Problems of Materials Science, National Academy of Sciences of Ukraine, Krjijanovskogo 3, 03142 Kyiv, Ukraine*

[3]*The Center for Nanophase Materials Sciences, Oak Ridge National Laboratory, Oak Ridge, Tennessee 37831, USA*

[4]*Taras Shevchenko Kyiv National University, Radiophysical Faculty, Prospect Akademika Hlushkova 4g, 03022 Kyiv, Ukraine*

[5]*Institute of Physics, National Academy of Sciences of Ukraine, Prospect Nauky 46, 03028 Kyiv, Ukraine*

[6]*Bogolyubov Institute for Theoretical Physics, National Academy of Sciences of Ukraine, 14-b Metrolohichna Street, 03680 Kyiv, Ukraine*

(Received 22 March 2017; revised manuscript received 14 July 2017; published 30 August 2017)

The *p-n* junction dynamics induced in a graphene channel by stripe-domain nucleation, motion, and reversal in a ferroelectric substrate is explored using a self-consistent approach based on Landau-Ginzburg-Devonshire phenomenology combined with classical electrostatics. Relatively low gate voltages are required to induce the hysteresis of ferroelectric polarization and graphene charge in response to the periodic gate voltage. Pronounced nonlinear hysteresis of graphene conductance with a wide memory window corresponds to high amplitudes of gate voltage. Also, we reveal the extrinsic size effect in the dependence of the graphene-channel conductivity on its length. We predict that the top-gate–dielectric-layer–graphene-channel–ferroelectric-substrate nanostructure considered here can be a promising candidate for the fabrication of the next generation of modulators and rectifiers based on the graphene *p-n* junctions.

DOI: 10.1103/PhysRevApplied.8.024027

I. INTRODUCTION

Since the discovery of graphene by Novoselov and Geim [1,2], its unique electronic, elastic, and optical properties [3,4] have been very attractive for the fundamental research of 2D semiconductors and promising for advanced application possibilities in modern nanoelectronics, optoelectronics, nanoplasmonics, sensors, and memory technologies. Following the development of graphene as a paradigm for 2D semiconductors, the remarkable properties of the *p-n* junction in graphene have been realized experimentally [5–7] and studied theoretically [8,9]. The first *p-n* junctions in graphene were realized by means of two-gate doping of one region with electrons and the other with holes [5]. The next *p-n* junction in a back-gated graphene channel was realized by a top gate superimposed on the dielectric layer above the channel [6]. For all of these cases [5–8,9], the resistance of *p-n* junction is quite low, since the electric field in the *p-n* junction is typically high due to the low screening ability of two-dimensional (2D) Dirac quasiparticles (electrons or holes). Several seminal studies of the *p-n* junctions' operation in graphene were devoted to the physical manifestations of Andreev reflection, Klein tunneling, quantum Hall effect, and Veselago lensing [10–12].

Remarkably, the usage of multiple-gate doping of a graphene channel by the opposite types of carriers is not the only possibility to design *p-n* junctions in graphene. The alternative promising and much less-explored way was not revealed until Hinnefeld *et al.* [13] and Baeumer *et al.* [14], who created a *p-n* junction in graphene using the ferroelectric substrates $Pb(Zr, Ti)O_3$ and $LiNiO_3$, respectively. Further, Baeumer *et al.* [14] considered the *p-n* junction induced in graphene by a ferroelectric-domain wall. The principal idea of the latter work is that if graphene is imposed on a 180° ferroelectric-domain wall, a *p-n* junction can arise without applying any additional gates, doping, or screening, due to the charge separation by an electric field of a ferroelectric-domain wall-surface junction. The physical origin of *p-n* junction appearance can be understood from the results of Zheng *et al.* [15] and Yusuf *et al.* [16], who decided to combine ferroelectrics with graphene, since a pronounced free-charge accumulation can take place at the graphene-ferroelectric interface [16]. Using the possibility of hysteretic ferroelectric gating, Zheng *et al.* [15] demonstrated a symmetrical bit writing in graphene-on-ferroelectric FETs with an electroresistance change of over 500%, as well as a reproducible, nonvolatile

*Corresponding author.
maksym.strikha@gmail.com
†Corresponding author.
anna.n.morozovska@gmail.com

switching. Recently, graphene-ferroelectric metadevices for nonvolatile memory and reconfigurable logic-gate operations have been proposed [17].

Kurchak and Strikha pointed out that adsorbed-charge dynamics leads to the unusual conductivity effects in the graphene channel on an organic ferroelectric substrate [18]. Morozovska *et al.* [19,20] have shown that the effective screening of the spontaneous polarization discontinuity at the ferroelectric surface by graphene free charge strongly decreases the electrostatic energy of the graphene-on-ferroelectric structures and can cause versatile phenomena, such as the charge-density modulation induced by the pyroelectric effect at the graphene-ferroelectric interface [19] and the triggering of the space-charge modulation in multilayer graphene by ferroelectric domains [20]. Finite-size effects can strongly influence the nonlinear hysteretic dynamics of the stored charge and electroresistance in the multilayer graphene-on-ferroelectric structures; in this case, the domain stripes of different polarities can induce domains with p- and n-type conductivity, and with p-n junction potentials [21]. A theoretical model for the electric field and ballistic transport in a single-layer graphene channel at a 180° ferroelectric-domain wall have been developed recently [22]. The results of Ref. [22] have been expanded for the case of different types of current regimes in Ref. [23]. In Ref. [23] we presented the theory of the conductivity of p-n junction in a graphene channel, placed on a ferroelectric substrate, caused by a ferroelectric-domain wall for the case of an arbitrary current regime—from a purely ballistic one to a diffusive one.

Here, complementary to Refs. [21–23], we consider the multidomain-state dynamics in a ferroelectric substrate. Using a self-consistent approach based on Landau-Ginzburg-Devonshire (LGD) phenomenology combined with classical electrostatics, here we study p-n junction dynamics induced in a graphene channel by stripe-domain nucleation, motion, and a reversal in a ferroelectric substrate. We suppose that 2D electrons in a single-layer graphene sheet have a Dirac density of states.

II. ANALYTICAL TREATMENT

A. Problem statement

The geometry of the considered problem is shown in Fig. 1(a). The top gate is deposited on the oxide layer; then the 2D graphene layer (channel) is separated from a ferroelectric substrate by an ultrathin paraelectric dead layer, which originates due the imperfect deposition process of graphene on the ferroelectric. The ferroelectric substrate is in ideal electric contact with the bottom-gate electrode. Periodic voltage is applied to the top gate. The voltage can induce a 180° ferroelectric-domain-wall (FDW) motion in the ferroelectric substrate.

A schematic of the p-n junction created in the graphene channel by domain walls moving in the ferroelectric substrate is shown in Fig. 1(b). Since the lateral dimension of a ferroelectric film L_{FE} is typically much higher than the graphene-channel length L, an odd, even. or fractional number of domain walls can pass along the channel during the period of the gate voltage depending on the interrelation between the graphene-channel length L and the period T_{FE} of the domain structure in a ferroelectric film.

Below, we describe how we model each of the layers in the heterostructure.

Single-layer graphene channel.—We treat a single-layer graphene as an infinitely thin sheet for which the 2D electron density of states is $g_n(\varepsilon) = g_p(\varepsilon) = 2\varepsilon/(\pi\hbar^2 v_F^2)$ (see, e.g., Ref. [24]). Hence, the 2D concentration of electrons in the

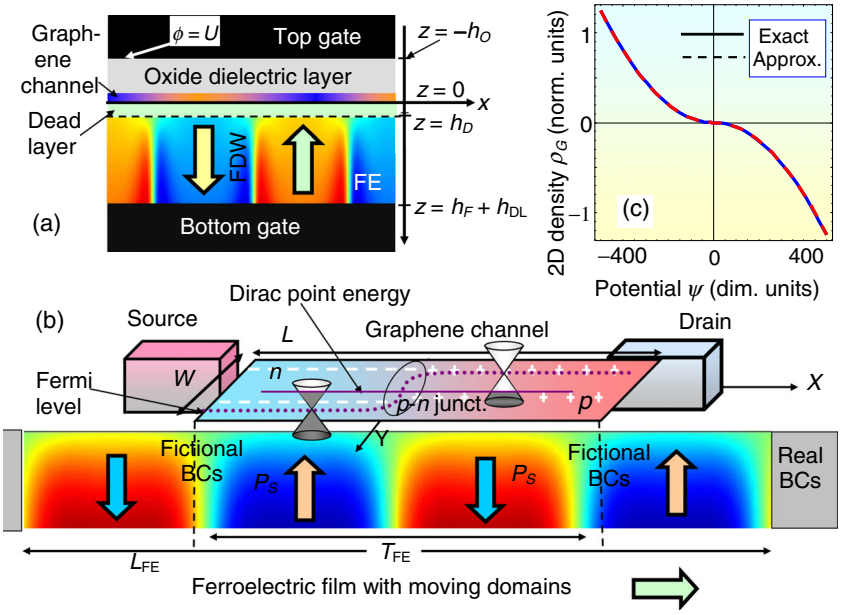

FIG. 1. (a) Schematics of the 180° domain wall structure near the ferroelectric surface in the heterostructure "top gate oxide dielectric layer graphene channel paraelectric dead layer ferroelectric film bottom gate." (b) Schematics of the p-n junction induced in the graphene channel by domain walls moving in the ferroelectric substrate. (c) Dependence of the 2D charge density of graphene on the dimensionless variable $\psi = [(e\phi + E_F)/k_BT]$. The solid curve is the exact expression (1); the dashed curve is the Pade-exponential approximation (2).

conduction band and holes in the valence band of graphene are $n_{2D}(\phi) = \int_0^\infty d\varepsilon g_n(\varepsilon) f(\varepsilon - E_F - e\phi)$ and $p_{2D}(\phi) = \int_0^\infty d\varepsilon g_p(\varepsilon) f(\varepsilon + E_F + e\phi)$, respectively ($E_F$ is a Fermi energy level; these expressions correspond the gapless graphene spectrum). For a pure planar graphene sheet we introduce a new variable $\psi = [(e\phi + E_F)/k_B T]$. Using the variable the graphene charge density $\sigma_G(\psi) = e[p_{2D}(\psi) - n_{2D}(\psi)]$ is equal to

$$\sigma_G(\psi) = \frac{2(k_B T)^2 e}{\pi\hbar^2 v_F^2}\{Li_2[-\exp(\psi)] - Li_2[-\exp(-\psi)]\}. \tag{1}$$

Here, $Li_n(z) = \sum_{m=1}^{\infty}[(z^m)/m^n]$ is the polylogarithm function (see Appendix A of the Supplemental Material [25]). The corresponding Pade-exponential approximation of Eq. (2) valid for arbitrary ψ values is

$$\sigma_G(\psi) \approx \frac{2(k_B T)^2 e}{\pi\hbar^2 v_F^2}\left(\frac{1}{\eta(\psi)} - \frac{1}{\eta(-\psi)}\right), \tag{2}$$

where the function $\eta(\psi) = \exp(\psi) + 2\{\psi^2 + (\psi/2) + [2\pi^2/(12 - \pi^2)]\}^{-1}$. Since the problem of dielectric permittivity of the 2D graphene layer is still under debate (see, e.g., Ref. [26]), our results obtained for the density of states from Eq. (1) are free from the problems inherent for 3D Boltzmann or Debye-Thomas-Fermi approximations [21,22].

Dielectric and dead layer.—Equations of state $\mathbf{D} = \varepsilon_0\varepsilon_O\mathbf{E}$ and $\mathbf{D} = \varepsilon_0\varepsilon_{DL}\mathbf{E}$ relate the electrical displacement $\mathbf{D}$ and electric field $\mathbf{E}$ in the oxide dielectric and ultrathin dead layers of thicknesses h_O and h_{DL}, respectively; ε_0 is a universal dielectric constant. Despite there being different types of "dead" (or "passive") layers [27,28], most of them are treated as ultrathin subsurface layers located under the surface of ferroelectric substrate, where the spontaneous polarization is absent (or negligibly small) due to the surface contamination, zero extrapolation length, and/or strong depolarization field [27,28]. The matter in the dead layer is of almost the same chemical composition as in the bulk of the ferroelectric substrate, but it is induced in the paraelectric phase by the surface confinement effect, and so the relative dielectric permittivity of the dead layer ε_{DL} is rather high, approximately 10^2 (as it should be for paraelectrics at room temperature [29]), in comparison with unity for a physical gap. The potential ϕ_{DL} satisfies Laplace's equation inside the dead layer.

Ferroelectric substrate.—As a substrate, we consider a ferroelectric film of thickness l with a ferroelectric polarization P_3^f directed along its polar axis z, with 180° domain-wall–surface junctions [see Fig. 1(a)]. Also, we assume that the dependence of polarization components on the inner field $\mathbf{E}$ can be linearized for transverse components as $P_1 = \varepsilon_0(\varepsilon_{11}^f - 1)E_1$ and $P_2 = \varepsilon_0(\varepsilon_{22}^f - 1)E_2$. Ferroelectric is dielectrically isotropic in transverse directions, i.e., the relative dielectric permittivity is equal, $\varepsilon_{11}^f = \varepsilon_{22}^f$. The polarization z component is $P_3(\mathbf{r}, E_3) = P_3^f(\mathbf{r}, E_3) + \varepsilon_0(\varepsilon_{33}^b - 1)E_3$, where a so-called relative "background" permittivity ε_{ij}^b is introduced [27]. The values of ε_{ij}^b are not related with a soft ferroelectric mode and limited by the linear dielectric response of the lattice, so for most of the ferroelectrics perovskites they are within the range of 4–7 (see Ref. [30] for its determination, and references therein). Hence, the ferroelectric permittivity ε_{33}^f related with the soft mode is much higher than the background, $\varepsilon_{33}^f \gg \varepsilon_{33}^b$. Inhomogeneous spatial distribution of the ferroelectric polarization $P_3(x, y, z)$ is determined from the time-dependent LGD-type Euler-Lagrange equation,

$$\Gamma\frac{\partial P_3}{\partial t} + aP_3 + bP_3^3 + cP_3^5 - g\Delta P_3 = E_3. \tag{3a}$$

Γ is a Landau-Khalatnikov relaxation coefficient [31], and g is a gradient coefficient, Δ stands for a 3D Laplace operator. Corresponding boundary conditions are of the third kind [32],

$$\left(P_3 - \Lambda_+\frac{\partial P_3}{\partial z}\right)\Big|_{z=h_D} = 0,$$
$$\left(P_3 + \Lambda_-\frac{\partial P_3}{\partial z}\right)\Big|_{z=h_{DL}+h_F} = 0. \tag{3b}$$

The physical range of extrapolation lengths $\Lambda_\pm$ is (0.5–2) nm [33]. Constants $a = \alpha_T(T - T_C)$, b, and c are the coefficients of LGD potential expansion on the polarization powers (also called linear and nonlinear dielectric stiffness coefficients). The quasistatic electric field is defined via electric potential as $E_3 = -\partial\phi/\partial z$. The potential ϕ_f satisfies the Poisson equation inside a ferroelectric film.

Also, we suppose that the polarization relaxation time $\tau_{LK} = \Gamma/|a_3| \sim 10^{-11}$ s is much higher than the graphene charge relaxation time $\tau_M = \varepsilon\varepsilon_0/(e\eta n_S) \sim 10^{-12}$ s (ε_0 is a universal dielectric constant, ε is a relative dielectric permittivity, η is a mobility of carriers in graphene), and so adiabatic approximation can be used for the charge description (see Fig. S1 in Appendix B of the Supplemental Material [25]). The inequality $\tau_{LK} \gg \tau_M$ works well in the vicinity of the ferroelectric phase transition, where τ_{LK} diverges due to the critical slowing-down effect.

Hence, for the problem geometry shown in Fig. 1(a), the system of electrostatic equations acquires the form

$$\Delta\phi_O = 0, \quad \text{for } -h_O < z < 0 \quad (\text{oxide dielectric layer } O), \tag{4a}$$

$$\Delta\phi_{DL} = 0, \quad \text{for } 0 < z < h_{DL} \quad (\text{dead layer DL}), \tag{4b}$$

$$\left(\varepsilon_{33}^{b}\frac{\partial^2}{\partial z^2}+\varepsilon_{11}^{f}\Delta_{\perp}\right)\phi_f=\frac{1}{\varepsilon_0}\frac{\partial P_3^f}{\partial z},$$
$$\text{for } h_{\mathrm{DL}}<z<h_{\mathrm{DL}}+h_F \quad (\text{ferroelectric } f). \tag{4c}$$

The 3D Laplace operator is Δ, the 2D Laplace operator is $\Delta_{\perp}$. Boundary conditions to the system (4) are the fixed potential at the top ($z=-h_O$) and bottom ($z=h_{\mathrm{DL}}+h_F\approx h_F$) gate electrodes; the continuity of the electric potential at the graphene layer ($z=0$) and the equivalence of difference of the electric displacement normal components, $D_3^O=\varepsilon_0\varepsilon_O E_3$ and $D_3^{\mathrm{DL}}=\varepsilon_0\varepsilon_{\mathrm{DL}}E_3$, to the surface charges in graphene $\sigma_G(x,y)$; and the continuity of the displacement normal components, $D_3^f=\varepsilon_0\varepsilon_{33}^b E_3+P_3^f$ and $D_3^{\mathrm{DL}}=\varepsilon_0\varepsilon_{\mathrm{DL}}E_3$, at the dead-layer–ferroelectric interface.

The explicit form of the boundary conditions (BCs) in the z direction is

$$\phi_O(x,y,-h_O)=U(t), \tag{5a}$$

$$\begin{aligned}\phi_O(x,y,0)&=\phi_{\mathrm{DL}}(x,y,0),\\ D_3^O(x,y,0)-D_3^{\mathrm{DL}}(x,y,0)&=\sigma_G(x,y),\end{aligned} \tag{5b}$$

$$\begin{aligned}\phi_d(x,y,h_{\mathrm{DL}})&=\phi_f(x,y,h_{\mathrm{DL}}),\\ D_3^{\mathrm{DL}}(x,y,h_{\mathrm{DL}})-D_3^f(x,y,h_{\mathrm{DL}})&=0,\end{aligned} \tag{5c}$$

$$\phi_f(x,y,h_{\mathrm{DL}}+h_F)=0. \tag{5d}$$

The gate voltage is periodic with a period T_g, $U(t)=U_{\max}\sin(2\pi t/T_g)$.

To generate moving domains, ferroelectric film thickness should be above the critical thickness l_{cr} of the size-induced phase transition into a paraelectric phase. The critical thickness of the single-domain ferroelectric state instability strongly depends on the dielectric and dead-layer thicknesses, namely [34], $l_{\mathrm{cr}}(T)\approx[1/\alpha_T(T_C-T)]\{[(2g)/\lambda+L_C]+[(h_{\mathrm{DL}})/\varepsilon_0\varepsilon_{\mathrm{DL}}]+[(h_O)/\varepsilon_0\varepsilon_O]\}$, where $L_C=\sqrt{g/\varepsilon_0\varepsilon_{33}^b}\sim 0.1$ nm is a correlation length in the z direction that is very small due to the depolarization field effect [35,36].

B. The "fictional" boundary conditions at the source and drain planes

The domain origins can be energetically favorable above the critical thickness, since they minimize the depolarization field energy in the gap and dielectric layer [37]. The period of domain stripes depends on the thicknesses of the oxide dielectric layer h_O, dead layer h_{DL}, and film h_F in a self-consistent way.

We note that exact domain dynamics will be determined by the interplay of the driving forces, memory effects in materials due to defects, and parity effects. Here, we consider only the latter, assuming no pinning on the top surface.

Contrary to the popular belief that the controlled motion of a solitary domain wall (or a small number of them) in a ferroelectric film under a channel is relatively easy to carry out, this task is hardly feasible for thin films, which have lateral surfaces $x=\pm L_{\mathrm{FE}}/2$ [designated "real BCs" in Fig. 1(b)] that border with air or solid. First of all, because these surfaces are themselves topological defects, on which a partial or complete pinning of the domain walls occurs, these walls can be "flipped" only hypothetically by applying a very large electrical voltage to the gate that is rather difficult in reality because of the electric breakdown of a thin oxide dielectric layer, as well as of a thin ferroelectric film. In addition, large fields in thin films do not agree with the requirements for energy saving and miniaturization of heterostructures. In reality, there are many domain stripes in a thin ferroelectric film, which expand or contract with the film polarization reversal, rather than a "domain" running along the film in a transverse direction. Thus, the motion, birth, or annihilation of domain walls inside the film is likely, in that the polarization values on the surfaces $x=\pm L_{\mathrm{FE}}/2$ are determined by the screening conditions and pinning centers. In this case, the domain walls naturally move along the channel, but sometimes towards each other.

In this case, it is reasonable to assume general boundary conditions of the third kind for polarization $P_3\pm\lambda_{\pm}^F(\partial P_3/\partial x)|_{x=\pm(L_{\mathrm{FE}}/2)}=0$, with different extrapolation lengths $\lambda_{\pm}^F$ at different lateral surfaces of the film $x=+L_{\mathrm{FE}}/2$ and $x=-L_{\mathrm{FE}}/2$. In general, the values of $\lambda_{\pm}^F$ are unknown, but, as a rule, they are regarded as not being negative (including special cases of zero and an infinitely large value) [32,33,35,37,38]. It turns out that for any positive $\lambda_{\pm}^F$ the domains expand and contract more often when a periodic voltage is applied to the film, rather than a solitary domain wall moves in the transverse direction. The equilibrium period of the domain structure is practically independent of the boundary conditions and is determined by the film thickness h_F, temperature, and screening conditions on its polar surface $z=h_{\mathrm{DL}}$ [37]. Since for a realistic situation $L_{\mathrm{FE}}\gg L_c$ (where $L_c\cong\sqrt{-a/g}$ is a correlation length that is the same order of lattice constant far from Curie temperature) and $L_{\mathrm{FE}}\gg L$, the solution for the polarization of the film "under" the channel (i.e., at $-L/2\le x\le L/2$) practically does not depend on the specific type of BCs at the surfaces $x=\pm L_{\mathrm{FE}}/2$. Taking into account that $L_{\mathrm{FE}}\gg L$, it is possible to perform calculations on a computational cell with a transverse dimension $-L/2\le x\le L/2$.

Since the lateral dimension of a ferroelectric film L_{FE} is typically much higher than the graphene-channel length L, an odd, even, or not fractional number of domain walls can pass along the channel during the period of the gate voltage T_g, depending on the interrelation between the

graphene-channel length L and the period T_{FE} of the domain structure in a ferroelectric film [Fig. 1(b)]. The realistic situations can be modeled by "fictional" boundary conditions (BCs) on the polarization component P_3, its derivative $\partial P_3/\partial x$, electric potential ϕ_f, and its derivative $\partial\phi_f/\partial x$ at the lateral boundaries $x = \pm L/2$ of the computation box $x = \pm L/2$, which will be listed below.

The periodic, antiperiodic, or mixed-parity BCs imposed on polarization and electric potential in the transverse x direction model the appearance and motion of different parity (*even* or *odd*, or *fractional*) of p-n junctions along the channel of length L over a voltage period, respectively. It appears that periodic BCs for polarization and potential, and their derivatives,

$$P_3\left(-\frac{L}{2},y,z\right) = P_3\left(+\frac{L}{2},y,z\right),$$
$$\left.\frac{\partial P_3}{\partial x}\right|_{x=-L/2} = \frac{\partial P_3}{\partial x}_{x=+L/2} \quad \text{(periodic)}, \tag{6a}$$

$$\phi_f\left(-\frac{L}{2},y,z\right) = \phi_f\left(+\frac{L}{2},y,z\right),$$
$$\left.\frac{\partial \phi_f}{\partial x}\right|_{x=-L/2} = \frac{\partial \phi_f}{\partial x}_{x=+L/2} \quad \text{(periodic)}, \tag{6b}$$

allow the motion of the even number of domain walls in the ferroelectric, and so the even number of p-n junctions are moving in the channel. Thus, the asymmetry of the graphene-channel conductance and rectification effect is absent in this case for the reasons discussed below.

In contrast, the mixed-parity BCs

$$P_3\left(-\frac{L}{2},y,z\right) = P_3\left(+\frac{L}{2},y,z\right),$$
$$\left.\frac{\partial P_3}{\partial x}\right|_{x=-L/2} = \frac{\partial P_3}{\partial x}_{x=+L/2} \quad \text{(periodic)}, \tag{7a}$$

$$\phi_f\left(-\frac{L}{2},y,z\right) = -\phi_f\left(+\frac{L}{2},y,z\right),$$
$$\left.\frac{\partial \phi_f}{\partial x}\right|_{x=-L/2} = -\frac{\partial \phi_f}{\partial x}_{x=+L/2} \quad \text{(antiperiodic)}, \tag{7b}$$

can lead to the asymmetry of the graphene-channel conductance and rectification effect, which will be demonstrated in the next section.

The completely antiperiodic BCs

$$P_3\left(-\frac{L}{2},y,z\right) = -P_3\left(+\frac{L}{2},y,z\right),$$
$$\left.\frac{\partial P_3}{\partial x}\right|_{x=-L/2} = -\frac{\partial P_3}{\partial x}_{x=+L/2} \quad \text{(antiperiodic)}, \tag{8a}$$

$$\phi_f\left(-\frac{L}{2},y,z\right) = -\phi_f\left(+\frac{L}{2},y,z\right),$$
$$\left.\frac{\partial \phi_f}{\partial x}\right|_{x=-L/2} = -\frac{\partial \phi_f}{\partial x}_{x=+L/2} \quad \text{(antiperiodic)}, \tag{8b}$$

can lead to the motion of the odd number of domain walls in the ferroelectric, and hence the odd number p-n junctions can move in the channel. The asymmetries of the graphene-channel conductance and rectification effect are possible in this case. The physical consequences of the BCs are described below.

One can try to understand the effect of the BCs induced on the graphene conduction kinetics by the moving domain walls using the analytical results [22,23] for a thermodynamic state as an instant "snapshot" at some moment in time. Because of the results [22,23], it is natural to expect that for the *even* number $(2k)$ of walls between source and drain electrodes of the graphene channel, its conductions G_+^{total} and G_-^{total} are the same for both polarities of the gate voltage

$$\frac{G_+^{\mathrm{total}}}{G_-^{\mathrm{total}}} = 1, \tag{9a}$$

because for each polarity there are k p-n junctions with conduction, given by Eq. (8) of [23] (electrons are tunneling trough the barrier), and k p-n junctions with conduction, given by Eq. (10) of [23] (electrons do not feel the barrier). For the *odd* number of the walls $2k+1$, Eq. (14) of Ref. [23] can be modified as

$$\frac{G_+^{\mathrm{total}}}{G_-^{\mathrm{total}}} = \frac{\beta(L+\lambda)+\lambda k(1+\beta)}{\beta(L+\lambda)+\lambda k(1+\beta)+\lambda}, \tag{9b}$$

where the factor β is equal to $\sqrt{\pi\alpha c/4\varepsilon_{33}^f v_F}$, λ is the electron mean free path, ε_{33}^f is the ferroelectric permittivity, v_F is the Fermi velocity of electrons in graphene, $\alpha = 1/137$ is fine structure constant, c is light velocity in vacuum.

For a pronounced diffusion regime of current $\beta L \gg \lambda$, and/or for the great number of the walls, $k \gg k_{\mathrm{cr}}$, where $k_{\mathrm{cr}} = 1 + [\beta L/(1+\beta)\lambda]$, the right-hand side in Eq. (9b) tends to unity [as in Eq. (9a)], and a conduction of the graphene channel is described by a well-known expression [9]:

$$G = \frac{\lambda(n_{2\mathrm{D}})}{L}\frac{2e^2}{\hbar\pi^{3/2}} w\sqrt{n_{2\mathrm{D}}}. \tag{10}$$

Here, w is the graphene-channel width, $n_{2\mathrm{D}}$ is the 2D charge concentration in the channel, determined by Eq. (1). The mean free path $\lambda(n_{2\mathrm{D}})$ depends on the concentration $n_{2\mathrm{D}}$. In particular, $\lambda(n_{2\mathrm{D}}) \sim \sqrt{n_{2\mathrm{D}}}$ for the scattering at ionized centers in the substrate and in the temperature range far from the Curie temperature [9]. Therefore, the conduction is a linear function of concentration in this case.

TABLE I Parameter designations and numerical values.

Parameter, constant, or value	Numerical value and dimensionality
Oxide dielectric thickness	$h_O = (4\text{–}10)$ nm
Dielectric (dead) layer thickness	$h_{\mathrm{DL}} = (0\text{–}4) \times 10^{-10}$ m
Ferroelectric film thickness	$h_F = (50\text{–}500)$ nm
Graphene-channel length	$L = (20\text{–}200)$ nm
Universal dielectric constant	$\varepsilon_0 = 8.85 \times 10^{-12}$ F/m
Permittivity of the dielectric layer	$\varepsilon_{\mathrm{DL}} = 100$ (typical range 10–300)
Ferroelectric permittivity of the ferroelectric film	$\varepsilon_{33}^f = 500$, $\varepsilon_{11}^f = \varepsilon_{22}^f = 780$ [$Pb(ZrTi)O_3$-like]
Background permittivity of the ferroelectric film	$\varepsilon_{11}^b = \varepsilon_{22}^b = \varepsilon_{33}^b = 4$ [$Pb(ZrTi)O_3$, $BaTiO_3$, or other ferroelectric perovskite]
Landau-Ginzburg-Devonshire potential coefficients	$\alpha_T = 2.66 \times 10^5$ C^{-2} mJ/K, $T_C = 666$ K ($PbZr_xTi_{1-x}O_3$, $x \approx 0.5$), $P_S^{\mathrm{bulk}} = (0.5\text{–}0.7)$ $\mathrm{C/m^2}$, $b = 1.91 \times 10^8$ $\mathrm{J\,C^{-4}\,m^5}$, $c = 8.02 \times 10^8$ $\mathrm{J\,C^{-6}\,m^9}$
Temperature	$T = 298$ K (room temperature)
Dielectric anisotropy of ferroelectric film	$\gamma = \sqrt{\varepsilon_{33}^f/\varepsilon_{11}^f} = 0.8$
Extrapolation length	$\Lambda_+ = \Lambda_- = \infty$
Plank constant	$\hbar = 1.056 \times 10^{-34}$ J s $= 6.583 \times 10^{-16}$ eV s
Fermi velocity of electrons in graphene	$v_F \approx 10^6$ m/s

III. NUMERICAL RESULTS AND DISCUSSION

Below, we present the results of the numerical modeling of problems (1)–(5). We study numerically the modulation of the graphene-channel conductance caused by a domain structure moving in a ferroelectric substrate. Parameters used in the calculations are listed in Table I.

For the enlisted parameters we get the factor $\beta = 0.185$, the product $\beta L \approx (4\text{–}400)$ nm for the channel length $L = (20\text{–}2000)$ nm, and $k_{\mathrm{cr}} = 1 + 0.16L/\lambda$. So that the ratio $G_+^{\mathrm{total}}/G_-^{\mathrm{total}}$ can be noticeably different from unity for $\lambda \geq 0.185L$ and domain-wall number $k \leq 1 + 0.16L/\lambda$.

The polarization component in the ferroelectric film P_3, variation of 2D concentration of free carriers in the graphene channel $\Delta n_G = (p_{2\mathrm{D}} - n_{2\mathrm{D}})$, and the effective conductance ratio $\Delta\eta(U_{\max}) = \{[\Delta n_G(+U_{\max})]/[\Delta n_G(-U_{\max})]\}$ were calculated in dependence on the gate voltage $U(t) = U_{\max}\sin(2\pi t/T_g)$. Results of the calculations are presented and analyzed in the next subsections.

A. Hysteresis loops of ferroelectric polarization and carrier concentration at low voltages

The hysteresis loops of the average polarization $P_3(U)$ and concentration variation $\Delta n_G(U)$ are shown in Figs. 2(a)–2(f). Only the steady regime is shown, for all the cases the transient process was cut off. Black, red, and magenta loops correspond to the different amplitudes of gate voltage $U_{\max} = (2, 5, 10)$ V. At relatively low voltages ($\leq$2 V for chosen material parameters) polarization and concentration loops of quasielliptic shape do not reveal any ferroelectric peculiarities [see black curves in Figs. 2(a)–2(f)]. This happens because the film state is polydomain, and the domain walls do not disappear with the gate voltage changing from $-U_{\max}$ to $+U_{\max}$, but they are moved by the electric field. Actually, the domain walls are moving to minimize the system energy when the voltage higher than the coercive one is applied to the top gate. Note that the domain-wall pinning effects, which can affect the coercive field, are not considered in our modeling.

With the increase of the gate-voltage amplitude $U_{\max}$ to (5–10) V, the domain walls start to collide and the domains with an opposite polarization orientation almost "annihilate" for definite periodic moments of time t, and then the polar state of the film with some degree of unipolarity partially restores [see red and magenta curves in Figs. 2(a)–2(c) and Videos 1–3]. The loops' asymmetry and rectification ratio is defined by the symmetry of the BCs.

1. Impact of periodic boundary conditions

Completely symmetric loops of polarization $P_3(U)$ and concentration $\Delta n_G(U)$ variation correspond to the periodic BCs [Figs. 2(a) and 2(d)]. The averaged amount of positive (holes) and negative (electrons) charges is equal to one another for the periodic BCs. The rectification effect is absent in the case of periodic BCs, since the effective ratio $\Delta\eta(U_{\max}) \equiv -1$ for all $U_{\max}$ [see Fig. 2(g)], because the even number of domain walls is moving in the ferroelectric substrate at any time [see Video 1].

A typical distribution of electric potential and polarization for periodic BCs proved that two domain walls separating three domains with "up" and "down" polarizations are present in the ferroelectric film [see Fig. 3(a)]. An example

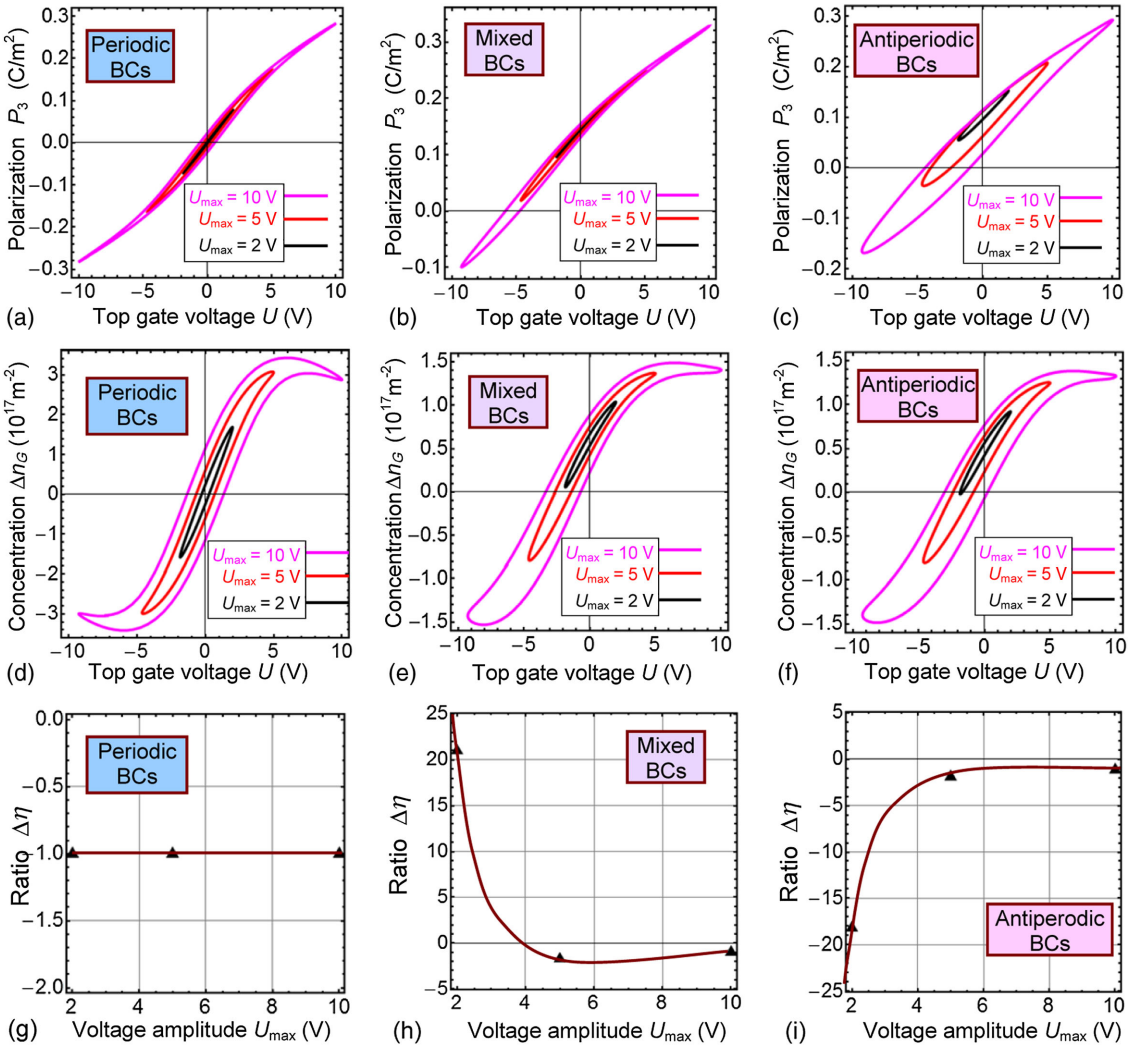

FIG. 2. Hysteresis loops of ferroelectric polarization $P_3(U)$ (a)–(c), carrier concentration variation in a graphene channel $\Delta n_G(U)$ (d)–(f) and the conductance ratio $\Delta\eta(U_{\max})$ (g)–(i) calculated for periodic (a),(d),(g), mixed (b),(e),(h), and antiperiodic (c),(f), (i) boundary conditions (BCs). Black, red, and magenta loops in plots (a)–(f) correspond to the different amplitudes of gate voltage $U_{\max} = (2, 5, 10)$ V. The thicknesses of ferroelectric film is $h_f = 75$ nm, oxide dielectric thickness $h_O = 8$ nm, dead-layer thickness $h_{\mathrm{DL}} = 0.4$ nm, gate-voltage period $T_g = 10^3$ s. Other parameters are listed in Table I. For animations of the ferroelectric-domain-structure evolution along one period of applied voltage, see Videos 1–3, corresponding to periodic, mixed, and antiperiodic BCs, respectively.

of the spatialtemporal evolution of the polarization component P_3 and corresponding free-charge concentration calculated along the graphene channel at certain times over a period is shown in Figs. 4(a) and 4(d), respectively. Two *p-n* junctions produced by the two moving domain walls are seen at certain times over one period. The relative depth (i.e., maximum-to-minimum ratio) and position ($\Delta n_G = 0$) of the *p-n* junctions are time dependent.

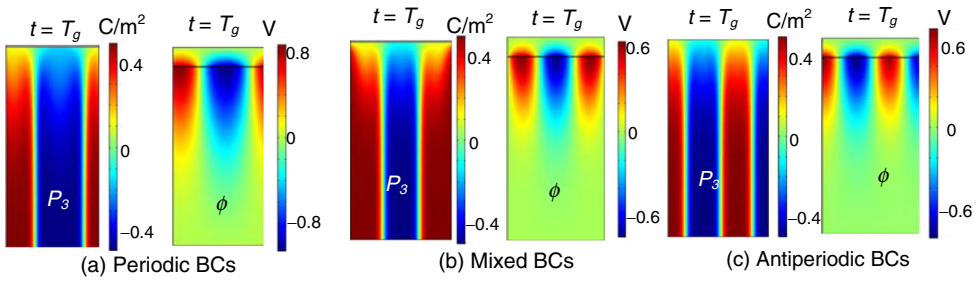

FIG. 3. Spatial distribution of a ferroelectric polarization component P_3 and electric potential ϕ calculated for the periodic (a), mixed (b), and antiperiodic (c) boundary conditions (BCs) at time $t = T_g$, $U_{\max} = 10$ V, and $T_g = 1000$ s. Other parameters are the same as in Fig. 2.

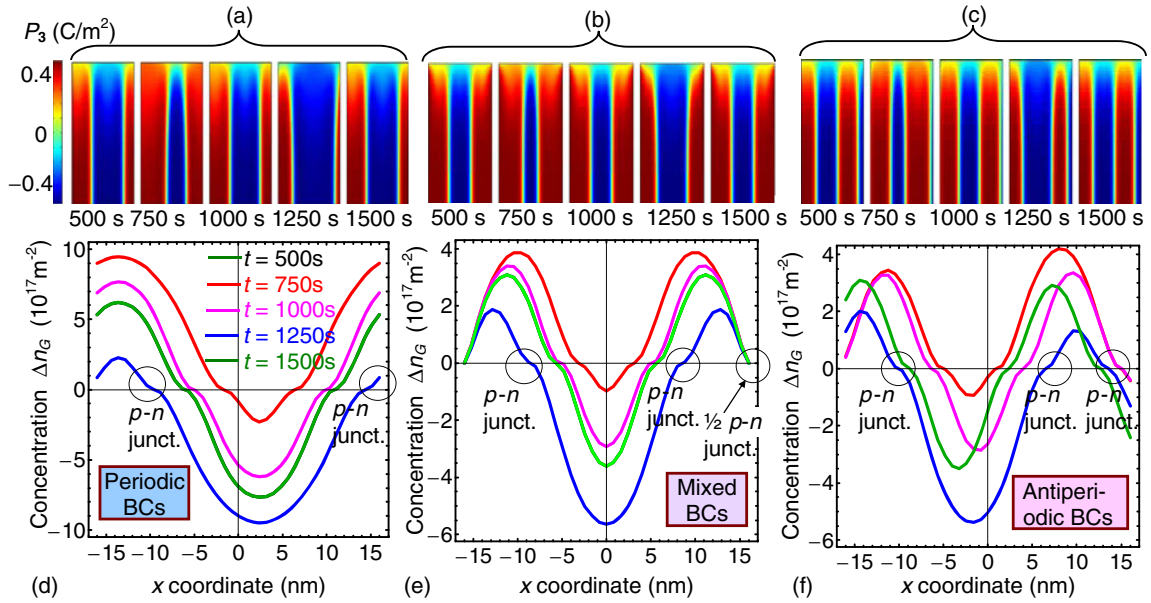

FIG. 4. Spatial distribution of polarization component P_3 in a ferroelectric film calculated at certain times over a period of 500, 750, 1000, 1250, and 1500 s (specified in the plots) for the periodic (a), mixed (b), and antiperiodic (c) BCs. 2D concentration of the free charge $\Delta n_G(x,t)$ calculated along the graphene channel at certain times over a period of 500, 750, 1000, 1250, and 1500 s (specified in the plots) for the periodic (d), mixed (e), and antiperiodic (f) BCs. Gate-voltage amplitude $U_{\max} = 5$ V and period $T_g = 10^3$ s. Other parameters are the same as in Fig. 2. The fast transient process is not shown (so that we started to show the plots from times $t \geq 500$ s).

Spatialtemporal distributions of 2D concentration of the free charge $\Delta n_G(x,t)$ calculated for the periodic BCs at a small amplitude of the gate voltage ($U_{\max} = 2$ V) is shown in Fig. 5(a). Maximal positive (holes) and negative (electrons) charge densities are equal to one another all the time for the periodic BCs [the corresponding color scale of the carrier density ranges from $+8.7 \times 10^{17}$ m^{-2} to -8.7×10^{17} m^{-2} in Fig. 5(a)], reflecting the fact that negative and positive polarizations are equivalent during the entire period for periodic BCs [see symmetric polarization loops in Fig. 2(a)].

2. Impact of mixed boundary conditions

Asymmetric loops of $P_3(U)$ and $\Delta n_G(U)$ correspond to the mixed BCs [Figs. 2(b) and 2(e)]. The vertical asymmetry and horizontal shift of the polarization loop are much stronger than the asymmetry of concentration variation because the polarization acts on the charge indirectly via the depolarization field. The asymmetry of $P_3(U)$ and $\Delta n_G(U)$ becomes weaker with a maximal voltage increase [compare the different loops in Figs. 2(b) and 2(e)]. The rectification effect is present in the case of low voltages, since the effective ratio $\Delta\eta(U_{\max}) \gg 1$ for $1\text{ V} < U_{\max} < 3$ V, the ratio changes sign at $U_{\max} = 4$ V, and then $\Delta\eta(U_{\max}) \to -1$ for higher voltages [see Fig. 2(h)], because asymmetric domain walls are moving in the ferroelectric film [see Video 2]. An instant distribution of the electric potential and polarization shows that two domain walls with a complex shape near the surface, which separate three domains (two with "up" and one with "down" polarizations), are located in the ferroelectric film [see Fig. 3(b)]. The spatialtemporal evolution of the polarization and corresponding free-charge concentration calculated along the graphene channel are shown in Figs. 4(b) and 4(e), respectively. Two *p-n* junctions produced by the two moving domain walls exist inside the channel at all times over one period. Also, there are two halves of "positive" *p-n* junctions at the channel boundaries and, most probably, these peculiarities create the asymmetry of the total conductance.

Spatialtemporal distributions of 2D concentration of the free charge $\Delta n_G(x,t)$ calculated for the mixed BCs are shown in Fig. 5(b). The charge-density symmetry is broken for the mixed BCs [the corresponding color scale ranges from $+3.6 \times 10^{17}$ m^{-2} to -4.4×10^{17} m^{-2} in Fig. 5(b)], reflecting the fact that polarization has a noticeable degree of unipolarity for the mixed BCs [see asymmetric polarization loops in Fig. 2(b)].

3. Impact of antiperiodic boundary conditions

The antiperiodic BCs also lead to asymmetric loops of polarization $P_3(U)$ and concentration $\Delta n_G(U)$ [Figs. 2(c) and 2(f)]. As in the previous case, the vertical asymmetry and horizontal shift of $P_3(U)$ loop are much stronger than the asymmetry of the $\Delta n_G(U)$ loop because the polarization acts on the charge indirectly via the depolarization field. The asymmetry of $P_3(U)$ and $\Delta n_G(U)$ becomes weaker with a maximal voltage increase [compare different

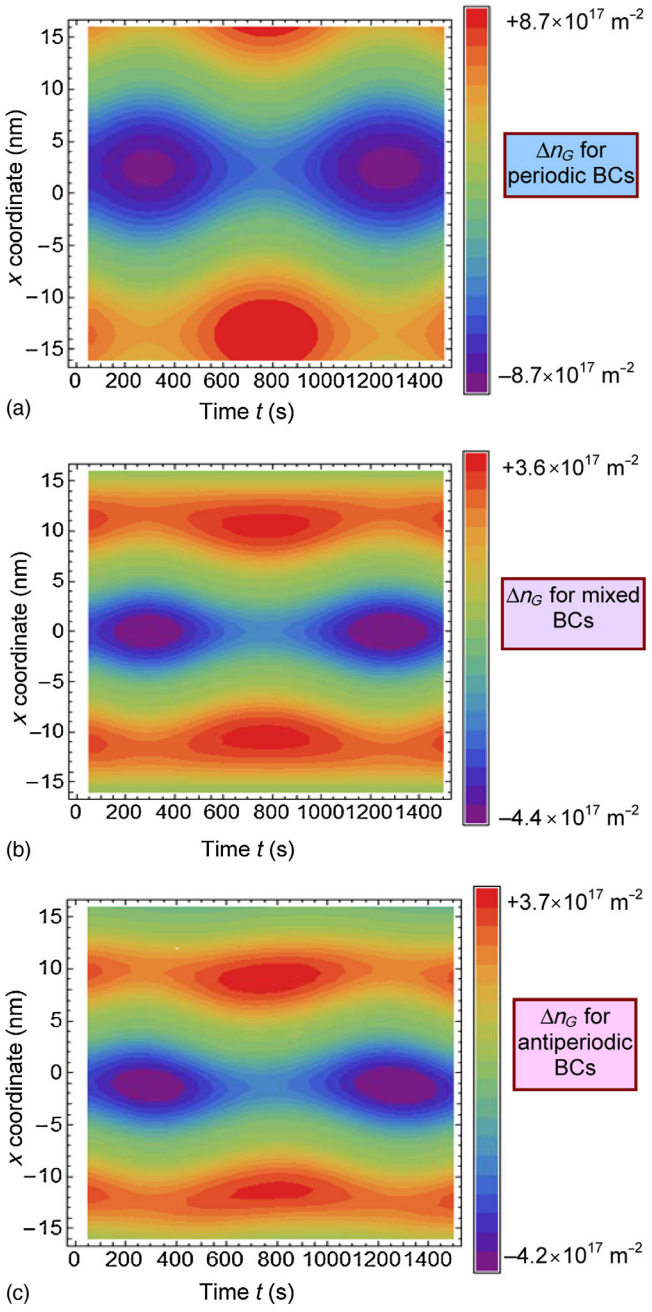

FIG. 5. Spatialtemporal distributions of 2D concentration of the free charge $\Delta n_G(x,t)$ calculated along the graphene channel for the periodic (a), mixed (b), and antiperiodic (c) BCs. Gate-voltage amplitude $U_{\max} = 2$ V and period $T_g = 1000$ s. Other parameters are the same as in Fig. 2.

loops in Figs. 2(c) and 2(f)]. The rectification effect is evident in the case of low and moderate voltages, since the effective ratio $\Delta\eta(U_{\max}) \ll 1$ for 1 V $< U_{\max} <$ 4 V, and for higher voltages then the ratio saturates, $\Delta\eta(U_{\max}) \to -1$ [see Fig. 2(i)], because the odd number of domain walls is moving in the ferroelectric film most of the time [see Video 3]. A typical distribution of electric potential and polarization show that three domain walls, which separate four domains (two with up and two with down polarizations), are present in the ferroelectric film [see Fig. 3(c)]. A typical spatialtemporal evolution of the polarization and corresponding graphene charge is shown in Figs. 4(c) and 4(f), respectively. Three p-n junctions produced by the three moving domain walls exist at almost all times over one period [see Video 3], and their relative depth and position are time dependent.

Spatialtemporal distributions of 2D concentration of the free charge $\Delta n_G(x,t)$ calculated for the antiperiodic BCs is shown in Fig. 5(c). The charge-density symmetry breaking for the antiperiodic BCs is evident from the figure, where the carrier density scale ranges from $+3.7 \times 10^{17}$ m^{-2} to -4.2×10^{17} m^{-2}, caused by the polarization asymmetry shown in Fig. 2(c).

Note that for low voltage amplitudes $U_{\max} < 10$ V, the maximal charge density $\sigma_G = e\Delta n_G \sim (0.024\text{–}0.048)$ C/m^2 recalculated from the $\Delta n_G \sim (1.5\text{–}3) \times 10^{17}$ m^{-2} appeared noticeably smaller than the spontaneous polarization of the ferroelectric film $P_S \sim 0.5$ C/m^2. This happens because of the electric potential drop in the oxide dielectric layer and corresponding appearance of the depolarization field in it.

To resume, the aperiodicity of electric boundary conditions for polarization at the lateral surfaces of the ferroelectric substrate can induce the voltage asymmetry of the graphene-channel conductance hysteresis loops.

B. Hysteresis loops of ferroelectric polarization and carrier concentration: Transition from low to high voltages

For comparative analysis of the system behavior at low, intermediate, and high gate voltages we calculate the dependences of domain-structure evolution and ferroelectric polarization in the substrate and the surface-charge concentration in a graphene channel on the gate voltage. Results for hysteresis loops of ferroelectric polarization $P_3(U)$ and surface-charge-concentration variation $\Delta n_G(U)$ are shown in Fig. 6 for periodic, mixed, and antiperiodic BCs, respectively. Black, brown, red, blue, and magenta loops correspond to the different amplitudes of gate voltage $U_{\max} = (2, 5, 10, 15, 20)$ V.

At relatively low voltages (less than 5 V for chosen material parameters) polarization and concentration loops of a quasielliptic shape look very slim for the chosen voltage window (20 V) and do not reveal any ferroelectric peculiarities [see red and brown curves in Fig. 6]. This happens because the film state is polydomain, and the domain walls do not disappear with the gate voltage changing from $-U_{\max}$ to $+U_{\max}$; they are moved in the electric field. With the increase of the gate-voltage amplitude $U_{\max}$ to (5–10) V the loops' shapes start to deviate from the elliptic one [compare red and brown curves in Fig. 6]. This happens because domain walls start to collide and the domains with opposite polarization orientation

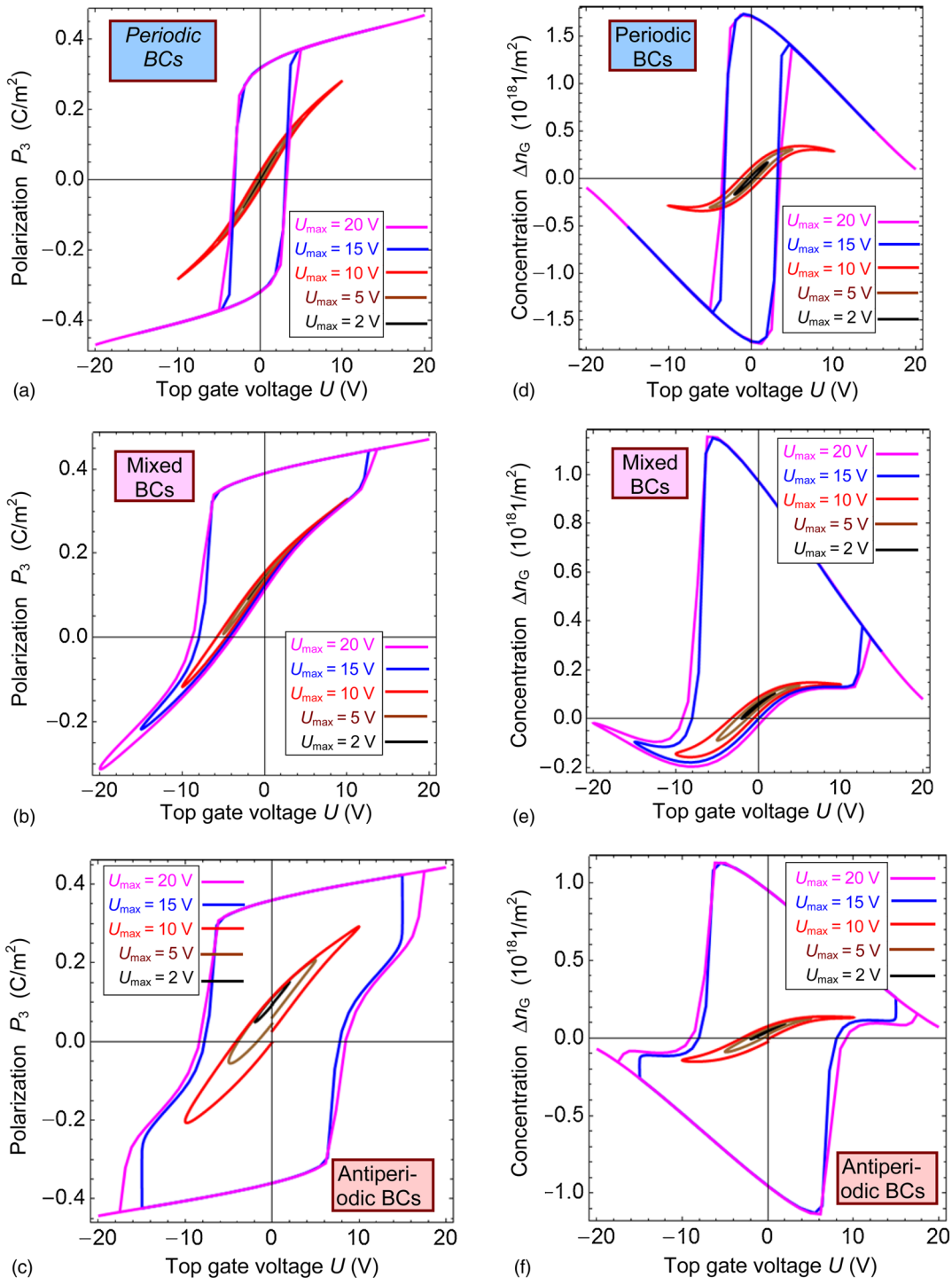

FIG. 6. Hysteresis loops of ferroelectric polarization (a)–(c) and surface-charge concentration in graphene channel (d)–(f) calculated in dependence on the gate voltage for periodic (a),(d), mixed (b),(d), and antiperiodic (c),(f) BCs. Black, brown, red, blue, and magenta loops correspond to the different amplitudes of gate voltage $U_{\max} = (2, 5, 10, 15, 20)$ V. The thicknesses of ferroelectric film $h_f = 75$ nm, oxide dielectric thickness $h_O = 8$ nm, dead-layer thickness $h_{\mathrm{DL}} = 0.4$ nm, gate-voltage period $T_g = 10^3$ s. Other parameters are listed in Table I.

almost "annihilate" for definite periodic moments of time t, and then the film polar state with a significant degree of unipolarity is partially restored. The degree of unipolarity strongly increases with the $U_{\max}$ increase to values higher than 10 V. We observe that the stationary switching regime is a single domain, independent of the polydomain seeding for $U_{\max} \geq 15$ V. Corresponding hysteresis loops undergo the voltage-induced phase transition with a $U_{\max}$ increase

above 10 V acquiring a pronounced loop opening with a high remnant polarization, charge, and coercive voltage (i.e., memory window) and a squarelike, irregular, or rhomboidal shape, depending on the BCs [compare blue and magenta loops with, e.g., red ones in Fig. 6].

Notice that for the voltages higher than 10 V one needs an especially good quality of dielectric layers, because the field in the oxide layer can be greater than the breakdown one (about 1 V/nm for SiO_2 [39]). Nevertheless, electric potential drops in the dielectric layer and gap, the graphene charge recalculated from the carrier concentration appears to be of the same order as the spontaneous polarization of the ferroelectric film at $U_{max} \geq 15$ V. This happens because the gate voltages are high enough to increase the polarization of the ferroelectric film during the entire period.

Symmetric square-shaped polarization loops with high coercive voltage correspond to the periodic BCs and voltage amplitude $U_{max} \geq 20$ V [see blue and magenta curves in Fig. 6(a)]. The modulation effect of the graphene carrier concentration loop is evident in this case and the rectification effect is absent [see blue and magenta curves in Fig. 6(d)], since an even number of domain walls are moving in the ferroelectric substrate. Spatial distributions of the domain structure in ferroelectric film below the channel along one period is demonstrated by Video 1.

Strongly asymmetric polarization loops with a high coercive voltage correspond to the mixed BCs and $U_{max} \geq 15$ V [see the blue and magenta curves in Fig. 6(b)]. The rectification effect of the carrier concentration loops with a pronounced memory window is evident in this case [see the blue and magenta curves in Fig. 6(e)]. Corresponding spatial distributions of the domain structure in ferroelectric film and the electric potential in the system calculated for different moments of time (500, 750, 1000, and 1250 s) are shown in Figs. 7(a) and 7(b), respectively. From Fig. 7(a), an odd number of domain walls are moving in the ferroelectric substrate.

Almost symmetric square-shaped polarization loops with a constriction, which have the highest coercive voltage, correspond to the antiperiodic BSc and $U_{max} \geq 15$ V [see the blue and magenta curves in Fig. 6(c)]. The carrier concentration loops have a rhombus shape with rounded corners and the highest coercive voltage in comparison with periodic and mixed BCs [see the blue and magenta curves in Fig. 6(f)]. In this case, the modulation effect of concentration is evident and the rectification effect is absent, since the switching process acquires an almost single-domain scenario at a high voltage amplitude and the fraction of the domain walls moving in the ferroelectric substrate becomes rather small. Hence, the loops' asymmetry inherent to the lower voltage amplitudes [see red curves in Figs. 6(c) and 6(f)] vanishes with U_{max} increasing to (15–20) V.

In contrast to the estimates made at the end of Sec. III A 3 for low voltages $U_{max} < 5$ V, at high voltages

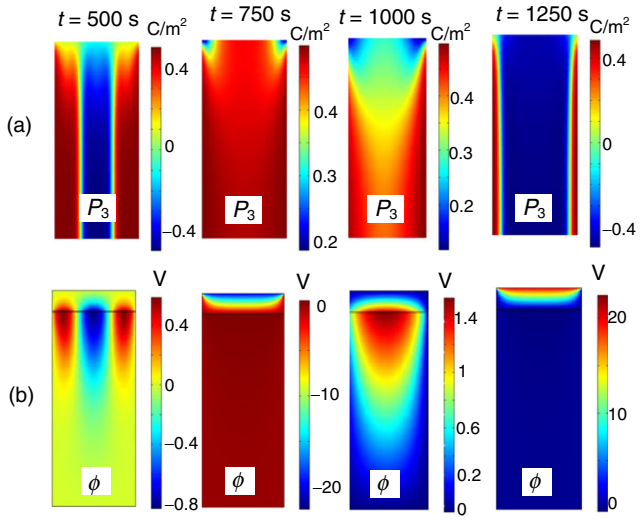

FIG. 7. Spatial distribution of ferroelectric polarization in P_3 in a ferroelectric film [(a), the top row] and electric potential ϕ [(b), the bottom row] calculated for the mixed BCs at $U_{max} = 20$ V for different moments of time (500, 750, 1000, and 1250 s). Other parameters are the same as in Fig. 6.

$U_{max} > 15$ V the maximal modulation of the graphene charge density $e\Delta n_G \sim (0.16\text{–}0.24)\,\mathrm{C/m^2}$ recalculated from the 2D concentration of carriers $\Delta n_G \sim (1-1.5)\times 10^{18}\,\mathrm{m^{-2}}$ appeared to be of the same order as the spontaneous polarization of the ferroelectric film $P_S \sim 0.5\ \mathrm{C/m^2}$.

C. Dependence of the graphene-channel conductivity on its length

Also, we reveal that the conductivity of the graphene channel [that is proportional to the total carrier concentration variation $\Delta n_G(L,t)$] depends on its length L in a rather nontrivial way. Corresponding contour maps of the average concentration variation $\Delta n_G(L,t)$ in coordinates "channel length L-time t" are shown in Fig. 8. The phenomenon we called "extrinsic size effect" consists of a quasiperiodic modulation of the conductivity amplitude with the channel length for periodic BCs, at which the modulation extremes are the most pronounced for L around 27.5 nm (the first maxima and minima depending on the time moment), 50 nm (the second maxima and minima), and slightly more than 70 nm (the third maxima and minima are not shown in the figure) at the parameters listed in Table I and room temperature. The modulation degree strongly increases with the gate-voltage amplitude increase above 5 V [compare Fig. 8(a) for $U_{max} = 5$ V with Fig. 8(b) for $U_{max} = 10$ V], but becomes less pronounced with an increase in L [compare the contrast for the modulation maxima and minima at $L = 27.5$ nm and 50 nm]. Also, the distance ΔL between the maxima is voltage independent and slightly increases with an increase in L [compare Fig. 8(a) with Fig. 8(b)].

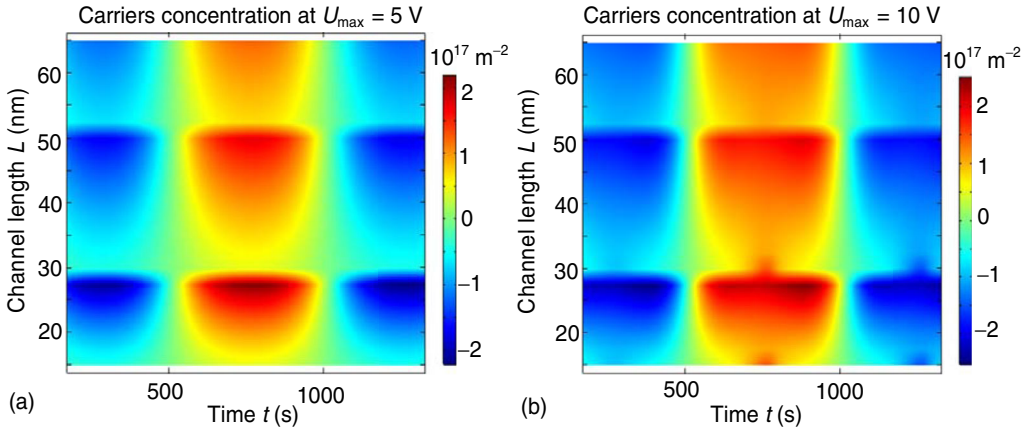

FIG. 8. Dependence of the graphene-channel conductivity on its length and time calculated for the periodic BCs at $U_{max} = 5$ V (a) and $U_{max} = 10$ V (b). Other parameters are the same as in Fig. 5.

Even though the peculiarities shown in Fig. 8 complicate the analytical treatment of the problem, we expect that the extrinsic size effect should vanish for long channels, whose length is much longer than the intrinsic period of domain structure in a ferroelectric substrate. Rigorously speaking, we relate the origin of the size effect with the interference of the domain-structure period and the channel length. Actually, the period of the 180° domain structure W is the intrinsic characteristic of the ferroelectric film that is defined by the film thickness, polarization screening conditions at the film-graphene and film–bottom gate interfaces ($z = 0$ and $z = h_F$), lateral surfaces ($x = +L_{FE}/2$ and $x = -L_{FE}/2$), surface energy (via extrapolation lengths $\Lambda_{\pm}$ and $\lambda_{\pm}^{F}$), and temperature [37]. Since the strong inequality $L_{FE} \gg L$ is regarded as being valid for the considered geometry, the period W becomes virtually independent of L_{FE} and extrapolation lengths $\lambda_{\pm}^{F}$, but the relation between W and L can be arbitrary (because L changes independently in Fig. 8); at that, the number of domains in the channel of length L is defined by two factors, the ratio L/W and the symmetry type of the virtual BCs at $x = \pm L/2$. As was established in Secs. II B and III A [see Eq. (9) and Figs. 2(d)–2(f)], since each of the domain walls creates a p-n junction in the graphene channel, the sign and values of the average concentration modulation $\Delta n_G(U,t)$ is defined by the total number k of the domain walls in the channel at low gate-voltage amplitudes $U_{max} \leq 10$ V. For a particular case of periodic BCs the number k should be even [see comments to Eq. (9a)]. Thus, the case when the integral part of the ratio L/W approaches an even number corresponds to the $\Delta n_G(U,t)$ extremes in Fig. 8, so that at low gate voltages the channel conductivity modulation naturally depends on the commensurability of the channel length L and the intrinsic period of the domain structure W. Allowing for the single-domain switching domination with the voltage increase the value of $\Delta n_G(U,t)$ is defined by the total degree of unipolarity of the ferroelectric substrate for the case of high voltages $U_{max} \geq 15$ V.

Note that extrinsic size effect can be expected for the mixed BCs. However, according to our additional calculations, its manifestation appears to be less pronounced and irregular than the one for the periodic (or antiperiodic) BCs. The result supports the interference origin of the size effect since the mixed BCs allow that a fractional number of the domain walls moving along the graphene channel and the commensurability of L and W are not required for the case.

To summarize the results of Sec. III, we predict that the top-gate–dielectric-layer–graphene-channel–ferroelectric-substrate nanostructure considered here can be a promising candidate for the fabrication of the next generation of modulators and rectifiers based on the graphene p-n junctions.

IV. CONCLUSION

Using a self-consistent approach based on Landau-Ginzburg-Devonshire phenomenology combined with classical electrostatics we study p-n junction dynamics induced in a graphene channel by stripe-domain nucleation, motion, and reversal in a ferroelectric substrate.

Relatively low amplitudes of gate voltages ($U_{max} \leq 5$ V) are required to induce the hysteresis of ferroelectric polarization and graphene charge in dependence on the periodic gate voltage. The harmoniclike charge-concentration modulation caused by a domain structure alternates with its homogeneous distribution caused by single-domain states under the periodic change of applied voltage.

Pronounced nonlinear hysteresis of graphene conductance with a wide memory window corresponds to high amplitudes of gate voltage $U_{max} \geq 15$ V, because the degree of unipolarity of the ferroelectric film strongly increases with a U_{max} increase and the stationary switching regime becomes a single domain independently of the polydomain seeding.

It was demonstrated that the asymmetry type of electric boundary conditions for polarization at the lateral surfaces of the ferroelectric substrate is responsible for the asymmetry of the hysteresis loop of graphene-channel conductance between the source and drain electrodes. In particular, asymmetric loops of polarization and charge

correspond to the mixed and antiperiodic boundary conditions. Completely symmetric loops of ferroelectric polarization and graphene charge-concentration variation correspond to the periodic boundary conditions.

For the periodic BCs we reveal the extrinsic size effect in the dependence of the graphene-channel L conductivity on its length that consists of a quasiperiodic modulation of the conductivity amplitude with L. The origin of the size effect can be related with the interference of the intrinsic period of the domain structure W and the channel length L. Namely, the conductivity extremes correspond to the situation when the integer part of the ratio L/W approaches an even number. The size effect can be expected for the mixed BCs, but its manifestation would be less pronounced than the one for the periodic (or antiperiodic) BCs, since the mixed BCs allow that a fractional number of the domain walls moving along the graphene channel and the commensurability of L and W are not required for the case. The result supports the interference origin of the size effect.

We expect that predicted effects become pronounced enough to be observed experimentally for the case of thin oxide dielectrics (<10 nm), intimate electric contact, or an ultrathin gap (<0.5 nm) between the ferroelectric and graphene sheet, short lengths of graphene channels (20–100) nm, and thin ferroelectric substrates (<100 nm). The first inequality mentioned above imposes demands for the dielectric with a high breakdown field. At that, it is extremely important to control the number of domain walls moving in the channel.

Taking into consideration the effects obtained in our work we predict that the top-gate–dielectric-layer–graphene-channel–ferroelectric-substrate nanostructure considered here can be a promising candidate for the fabrication of the next generation of modulators and rectifiers based on the graphene p-n junctions.

The Department of Energy will provide public access to these results of federally sponsored research in accordance with the DOE Public Access Plan [40].

ACKNOWLEDGMENTS

The authors are very grateful to Dr. Qian Li for useful suggestions. The publication contains the results of studies (A. I. K., E. A. E., A. N. M.) conducted by President's of Ukraine grant for competitive projects (Grant No. F74/25879) of the State Fund for Fundamental Research. S. V. K. acknowledges the Office of Basic Energy Sciences, U.S. Department of Energy. Part of the work was performed at the Center for Nanophase Materials Sciences, which is a DOE Office of Science User Facility.

A. I. K. and E. A. E. performed numerical calculations and made the figures. M. V. S. generated the research idea and motivation, derived analytical expression for graphene conductance, strongly contributed to the analysis of the results and manuscript improvement. S. V. K. contributed to the interpretation of the results and manuscript writing. A. N. M. formulated the problem mathematically, performed most of the analytical calculations, selected parameters, and wrote the manuscript.

APPENDIX: EVOLUTION OF DOMAIN STRUCTURE

Animations of the ferroelectric-domain-structure evolution along one period of applied voltage are demonstrated by Videos 1–3, corresponding to periodic, mixed, and antiperiodic BCs, respectively. Each image is obtained by calculating at specific time intervals within a period.

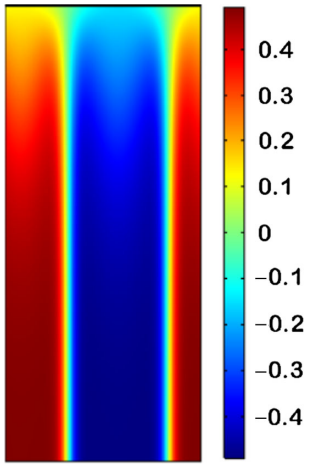

VIDEO 1. Animations of the ferroelectric-domain-structure evolution along one period of applied voltage for periodic BCs. Gate-voltage amplitude $U_{\max} = 10$ V and period $T_g = 10^3$ s. Other parameters are the same as in Fig. 2.

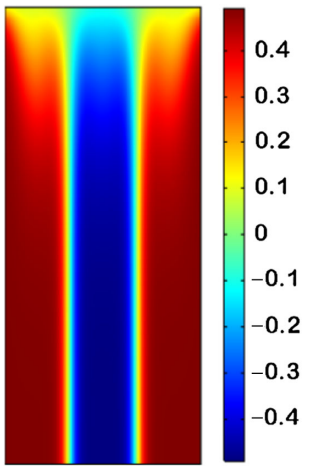

VIDEO 2. Animations of the ferroelectric-domain-structure evolution along one period of applied voltage for mixed BCs. Gate-voltage amplitude $U_{\max} = 10$ V and period $T_g = 10^3$ s. Other parameters are the same as in Fig. 2.

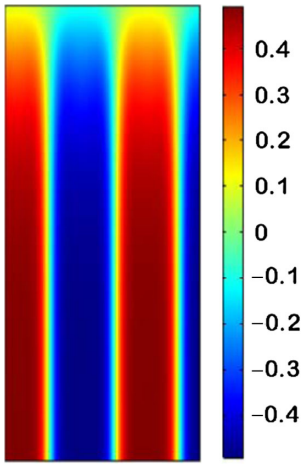

VIDEO 3. Animations of the ferroelectric-domain-structure evolution along one period of applied voltage for antiperiodic BCs. Gate-voltage amplitude $U_{\max} = 10\,\mathrm{V}$ and period $T_g = 10^3\,\mathrm{s}$. Other parameters are the same as in Fig. 2.

[1] K. Novoselov, A. Geim, S. Morozov, D. Jiang, Y. Zhang, S. Dubonos, I. Grigorieva, and A. Firsov, Electric field effect in atomically thin carbon films, Science **306**, 666 (2004).

[2] A. Geim, Graphene: Status and prospects, Science **324**, 1530 (2009).

[3] S. Das Sarma, Shaffique Adam, E. H. Hwang, and E. Rossi, Electronic transport in two-dimensional graphene, Rev. Mod. Phys. **83**, 407 (2011).

[4] Gerardo G. Naumis, Salvador Barraza-Lopez, Maurice Oliva-Leyva, and Humberto Terrones, Electronic and optical properties of strained graphene and other strained 2D materials: A review, arXiv:1611.08627 [Rep. Prog. Phys. (to be published)].

[5] V. Cheianov and V. Falko, Selective transmission of Dirac electrons and ballistic magnetoresistance of *n*-*p* junctions in graphene, Phys. Rev. B **74**, 041403 (2006).

[6] J. R. Williams, L. DiCarlo, and C. M. Marcus, Quantum Hall effect in a gate-controlled *p*-*n* junction of graphene, Science **317**, 638 (2007).

[7] J. R. Whyte and J. M. Gregg, A diode for ferroelectric domain-wall motion, Nat. Commun. **6**, 7361 (2015).

[8] N. M. Zhang and M. M. Fogler, Nonlinear Screening and Ballistic Transport in a Graphene *p*-*n* Junction, Phys. Rev. Lett. **100**, 116804 (2008).

[9] Yu. A. Kruglyak and M. V. Strikha, Generalized Landauer-Datta-Lundstrom model in application to transport phenomena in graphene, Ukr. J. Phys. Rev. **10**, 3 (2015).

[10] C. W. Beenakker, Andreev reflection and Klein tunneling in graphene, Rev. Mod. Phys. **80**, 1337 (2008).

[11] M. I. Katsnelson, K. S. Novoselov, and A. K. Geim, Chiral tunnelling and the Klein paradox in graphene, Nat. Phys. **2**, 620 (2006).

[12] V. V. Cheianov, V. I. Falko, and B. L. Altshuler, The focusing of electron flow and a Veselago lens in graphene *p*-*n* junctions, Science **315**, 1252 (2007).

[13] J. H. Hinnefeld, Ruijuan Xu, S. Rogers, Shishir Pandya, Moonsub Shim, L. W. Martin, and N. Mason, Single gate *p*-*n* junctions in graphene-ferroelectric devices, Appl. Phys. Lett. **108**, 203109 (2016).

[14] C. Baeumer, D. Saldana-Greco, J. M. P. Martirez, A. M. Rappe, M. Shim, and L. W. Martin, Ferroelectrically driven spatial carrier density modulation in graphene, Nat. Commun. **6**, 6136 (2015).

[15] Yi Zheng, Guang-Xin Ni, Chee-Tat Toh, Chin-Yaw Tan, Kui Yao, and Barbaros Özyilmaz, Graphene Field-Effect Transistors with Ferroelectric Gating, Phys. Rev. Lett. **105**, 166602 (2010).

[16] M. Humed Yusuf, B. Nielsen, M. Dawber, and X. Du, Extrinsic and intrinsic charge trapping at the graphene/ferroelectric interface, Nano Lett. **14**, 5437 (2014).

[17] Woo Young Kim, Hyeon-Don Kim, Teun-Teun Kim, Hyun-Sung Park, Kanghee Lee, Hyun Joo Choi, Seung Hoon Lee, Jaehyeon Son, Namkyoo Park, and Bumki Min, Graphene-ferroelectric metadevices for nonvolatile memory and reconfigurable logic-gate operations, Nat. Commun. **7**, 10429 (2016).

[18] A. I. Kurchak and M. V. Strikha, Conductivity of graphene on ferroelectric PVDF-TrFE, Ukr. J. Phys. **59**, 622 (2014).

[19] A. N. Morozovska and M. V. Strikha, Pyroelectric origin of the carrier density modulation at graphene-ferroelectric interface, J. Appl. Phys. **114**, 014101 (2013).

[20] A. N. Morozovska, E. A. Eliseev, A. V. Ievlev, O. V. Varenyk, A. S. Pusenkova, Ying-Hao Chu, V. Ya. Shur, M. V. Strikha, and S. V. Kalinin, Ferroelectric domain triggers the charge modulation in semiconductors, J. Appl. Phys., **116**, 066817 (2014).

[21] A. N. Morozovska, A. S. Pusenkova, O. V. Varenyk, S. V. Kalinin, E. A. Eliseev, and M. V. Strikha, Finite size effects of hysteretic dynamics in multi-layer graphene on ferroelectric, Phys. Rev. B **91**, 235312 (2015).

[22] Anna N. Morozovska, Eugene A. Eliseev, and Maksym V. Strikha, Ballistic conductivity of graphene channel with *p*-*n* junction on ferroelectric domain wall, Appl. Phys. Lett. **108**, 232902 (2016).

[23] Maksym V. Strikha and Anna N. Morozovska, Limits for the graphene on ferroelectric domain wall *p*-*n*-junction rectifier for different regimes of current, J. Appl. Phys. **120**, 214101 (2016).

[24] P. Nemes-Incze, Z. Osváth, K. Kamarás, and L. P. Biró, Anomalies in thickness measurements of graphene and few layer graphite crystals by tapping mode atomic force microscopy, Carbon **46**, 1435 (2008).

[25] See Supplemental Material at http://link.aps.org/supplemental/10.1103/PhysRevApplied.8.024027 for the derivation of the charge density and temperature dependences of the relaxation times.

[26] Elton J. G. Santos, in *Exotic Properties of Carbon Nanomatter* (Springer Dordrecht, Netherlands, 2015), pp. 383–391.

[27] A. K. Tagantsev and G. Gerra, Interface-induced phenomena in polarization response of ferroelectric thin films, J. Appl. Phys. **100**, 051607 (2006).

[28] A. K. Tagantsev, M. Landivar, E. Colla, and N. Setter, Identification of passive layer in ferroelectric thin films from their switching parameters, J. Appl. Phys. **78**, 2623 (1995).

[29] G. Rupprecht and R. O. Bell, Dielectric constant in paraelectric perovskite, Phys. Rev. **135**, A748 (1964).
[30] J. Hlinka and P. Márton, Phenomenological model of a 90° domain wall in $BaTiO_3$-type ferroelectrics, Phys. Rev. B **74**, 104104 (2006).
[31] L. D. Landau and I. M. Khalatnikov, On the anomalous absorption of sound near a second order phase transition point, Dokl. Akad. Nauk SSSR **96**, 469 (1954).
[32] R. Kretschmer and K. Binder, Surface effects on phase transitions in ferroelectrics and dipolar magnets, Phys. Rev. B **20**, 1065 (1979).
[33] Chun-Lin Jia, Valanoor Nagarajan, Jia-Qing He, Lothar Houben, Tong Zhao, Ramamoorthy Ramesh, Knut Urban, and Rainer Waser, Unit-cell scale mapping of ferroelectricity, and tetragonality in epitaxial ultrathin ferroelectric films, Nat. Mater. **6**, 64 (2007).
[34] Anna N. Morozovska, Eugene A. Eliseev, Nicholas V. Morozovsky, and Sergei V. Kalinin, Ferroionic states in ferroelectric thin films, Phys. Rev. B **95**, 195413 (2017).
[35] E. A. Eliseev and A. N. Morozovska, General approach to the description of the size effect in ferroelectric nanosystems, J. Mater. Sci. **44**, 5149 (2009).
[36] A. N. Morozovska, E. A. Eliseev, S. V. Svechnikov, A. D. Krutov, V. Y. Shur, A. Y. Borisevich, P. Maksymovych, and S. V. Kalinin, Finite size and intrinsic field effect on the polar-active properties of ferroelectric semiconductor heterostructures, Phys. Rev. B **81**, 205308 (2010).
[37] A. K. Tagantsev, L. E. Cross, and J. Fousek, *Domains in Ferroic Crystals and Thin Films.* (Springer, New York, 2010).
[38] D. R. Tilley, in *Ferroelectic Thin Films*, edited by C. Paz de Araujo, J. F. Scott, and G. W. Teylor (Gordon and Breach, Amsterdam, 1996), p. 11.
[39] M. V. Strikha, Non-volatile memory, and IR radiation modulators based upon graphene-on-ferroelectric substrate, A review, Ukr. J. Phys. Opt., Suppl. 3, **13**, S5 (2012).
[40] http://energy.gov/downloads/doe-public-access-plan.